

# Large-Scale Structure in the Universe

NETA A. BAHCALL

Princeton University Observatory, Princeton, NJ

## Abstract

How is the universe organized on large scales? How did this structure evolve from the unknown initial conditions to the present time? The answers to these questions will shed light on the cosmology we live in, the amount, composition and distribution of matter in the universe, the initial spectrum of density fluctuations, and the formation and evolution of galaxies, clusters of galaxies, and larger scale structures.

I review observational studies of large-scale structure, describe the peculiar velocity field on large scales, and present the observational constraints placed on cosmological models and the mass density of the universe. While major progress has been made over the last decade, most observational problems in the field of large-scale structure remain open. I will highlight some of the unsolved problems that seem likely to be solved in the next decade.

## 1. Introduction

The existence of large-scale structure in the universe has been known for over half a century (e.g., 49, 62). A spectacular increase in our understanding of this subject has developed over the last decade, led by observations of the distribution of galaxies and of clusters of galaxies. With major surveys underway, the next decade will provide new milestones in the study of large-scale structure. I will highlight what we currently know about large-scale structure, emphasizing some of the unsolved problems and what we can hope to learn in the next ten years.

Why study large-scale structure? We all want to know what the “skeleton” of our universe is, that is, how does the universe look on the largest scales we can investigate? It is natural to ask: on what scales does the universe become homogeneous and isotropic, as expected from the cosmological principle? In addition, we shall see that detailed knowledge of the large-scale structure provides constraints on:

- the formation and evolution of galaxies and larger structures;

- the cosmological model of our universe (including the mass density of the universe, the nature and amount of the dark matter, and the initial spectrum of fluctuations that gave rise to the structures seen today).

What have we learned so far, and what are the main unsolved problems in the field of large-scale structure? I discuss these questions in the sections that follow. I first list some of the unsolved problems.

There are many fundamental problems on which progress is likely to be made in the next decade. In fact, as we go through what is known about large-scale structure, you will see that most of what we want to know is a challenge for the future. Here is a partial list of some of the most interesting unsolved problems.

- Quantify the measures of large-scale structure. How large are the largest coherent structures? How strong is the clustering on large scales (e.g., as quantified by the power spectrum and the correlation functions of galaxies and other systems)?
- What is the topology of large-scale structure? What are the shapes and morphologies of superclusters, voids, filaments, and their networks?
- How does large-scale structure depend on galaxy type, luminosity, surface brightness? How does the large-scale distribution of galaxies differ from that of other systems (e.g., clusters, quasars)?
- What is the amplitude of the peculiar velocity field as a function of scale?
- What is the amount of mass and the distribution of mass on large scales?
- Does mass trace light on large scales? What is in the “voids”?
- What is the mass density,  $\Omega_m \equiv \rho_m / \rho_{\text{crit}}$ , of the universe?
- What is the baryon fraction of the universe,  $\Omega_b / \Omega_m$ ?
- How does the large-scale structure evolve with time?
- What are the implications of the observed large-scale structure for the cosmological model of our universe and for structure formation? (e.g., What is the nature of the dark matter? Does structure form by gravitational instability? What is the initial spectrum of fluctuations that gave rise to the structure we see today? Were the fluctuations Gaussian?)

Two-dimensional surveys of the universe analyzed with correlation function statistics 31, 39 reveal structure to scales of at least  $\sim 20h^{-1}$  Mpc. Large redshift surveys of the galaxy distribution reveal a considerably more detailed structure of superclusters, voids, and filament network extending to scales of  $\sim 50\text{--}100h^{-1}$  Mpc (29, 30, 16, 28, 22, 19, 27). The most recent and largest redshift survey, the Las Campanas Redshift Survey (35; see also 36), is presented in Figure 1; it reveals the “cellular” nature of the large-scale galaxy distribution. The upcoming Sloan Digital Sky Survey (SDSS), expected to begin operation in 1997 (see § 6), will provide a three dimensional map of the entire high-latitude northern sky to  $z \sim 0.2$ , with redshifts for approximately  $10^6$  galaxies. Figure 2 presents a simulation of one expected redshift slice from the SDSS survey; the slice represents  $\sim 6\%$  of the total survey. This survey, and others currently planned, will provide the large increase in the survey volume required to resolve some of the unsolved problems listed above (see § 6 for details).

One of the exciting new developments in the last decade is the ability to compare the large-scale observations with expectations from different cosmologies using state-of-the-art numerical cosmological simulations [see the contribution by J. P. Ostriker in these proceedings]. Standard cosmological models generally succeed in reproducing the overall large-scale structure that we observe. In Figure 3, I present two examples of the observed versus simulated redshift cone diagrams (the latter for a cold-dark-matter, CDM, model). I leave it up to the viewer to decide which figure displays data and which displays a simulation, and how well they match. The “good” news is that a simple cosmological model, starting from a rather uniform distribution of matter after the big-bang, with minute density fluctuations as prescribed by a CDM power spectrum [see the presentations by J. P. Ostriker, P. J. E. Peebles, and P. Steinhardt], can represent the universe we see today reasonably well. This is a real success for cosmology! The “bad” news is that the quantitative match with the simplest standard models is not very good. Model parameters need to be adjusted, some in an ad-hoc manner, in order to fit the data quantitatively.

## 2. Clustering and Large-Scale Structure

I summarize in Section 2.1 the ways that individual galaxies reveal the large-scale structure of the universe and describe in Section 2.2 the study of large-scale structure using clusters of galaxies.

## 2.1. Galaxies and Large-Scale Structure

The correlation function (of galaxies, of clusters of galaxies, of quasars) is a powerful statistical measure of the clustering strength on different scales. The two-point spatial correlation function,  $\xi(r)$ , is the net probability above random of finding a pair of objects, each within a given volume element  $dV_i$ , separated by the distance  $r$ . The total probability of finding such a pair is given by:

$$dP = n^2(1 + \xi(r))dV_1dV_2 , \quad (1)$$

where  $n$  is the mean density of objects in the sample.

The angular (projected) galaxy correlation function was first determined from the 2D Lick survey and inverted into a spatial correlation function by Groth & Peebles 31. They find  $\xi_{gg}(r) \simeq 20r^{-1.8}$  for  $r \lesssim 15h^{-1}$  Mpc, with correlations that drop to the level of the noise for larger scales. This observation implies that galaxies are clustered on at least  $\lesssim 15h^{-1}$  Mpc scale, with a correlation scale of  $r_o(gg) \simeq 5h^{-1}$  Mpc, where  $\xi(r) \equiv (r/r_o)^{-1.8} \equiv Ar^{-1.8}$ . More recent results support the above conclusions (with possibly a weak tail to larger scales in the galaxy correlations). One of the recent determinations of the two-point angular galaxy correlation function, using the APM 2D galaxy survey 39, 23, is presented in Figure 4. The observed correlation function is compared with expectations from the CDM cosmology (using linear theory estimates) for different values of the parameter  $\Gamma = \Omega_m h$ . Here  $\Omega_m$  is the mass density of the universe in terms of the critical density and  $h \equiv H_0/100 \text{ km s}^{-1} \text{ Mpc}^{-1}$  [see the contribution of Peebles]. The different  $\Omega_m h$  models differ mainly in the large-scale tail of the galaxy correlations: higher values of  $\Omega_m h$  predict less structure on large scales (for a given normalization of the initial mass fluctuation spectrum) since the CDM fluctuation spectrum (see below) peaks on scales that are inversely proportional to  $\Omega_m h$ . It is clear from Figure 4, as was first shown from the analysis of galaxy clusters (see below), that the standard CDM model with  $\Omega_m = 1$  and  $h = 0.5$  does not produce enough large-scale power to match the observations. As Figure 4 shows, the galaxy correlation function requires  $\Omega_m h \sim 0.15\text{--}0.2$  for a CDM-type spectrum, consistent with other large-scale structure data.

The power spectrum,  $P(k)$ , which reflects the initial spectrum of fluctuations [see the discussion by P. Steinhardt in these proceedings] that gave rise to galaxies and other structure, is represented by the Fourier transform of the correlation function (e.g., 45). One of the recent attempts to determine this fundamental statistic using a variety of tracers is presented in Figure 5 (42; see also 56, 24, 41, 36). The determination of this composite spectrum assumes different normalizations for the different tracers used (optical galaxies, IR galaxies, clusters of galaxies). The different normalizations imply a different bias parameter  $b$  for each of the different tracers [where  $b \equiv (\Delta\rho/\rho)_{\text{gal}}/(\Delta\rho/\rho)_m$  represents the overdensity

of the galaxy tracer relative to the mass overdensity]. Figure 5 also shows the microwave background radiation (MBR) anisotropy as measured by COBE 50 on the largest scales ( $\sim 1000h^{-1}$  Mpc) and compares the data with the mass power spectrum expected for two CDM models: a standard CDM model with  $\Omega_m h = 0.5$  ( $\Omega_m = 1, h = 0.5$ ), and a low-density CDM model with  $\Omega_m h = 0.25$ . The latter model appears to provide the best fit to the data, given the normalizations used by the authors for the different galaxy tracers.

The next decade will provide critical advances in the determination of the correlation function and the related power spectrum. The large redshift surveys now underway (§ 6) will probe the power spectrum of galaxies to larger scales than currently available and with greater accuracy. These surveys will bridge the gap between the current optical determinations of  $P(k)$  of galaxies on scales  $\lesssim 100h^{-1}$  Mpc and the MBR anisotropy on scales  $\gtrsim 10^3h^{-1}$  Mpc. This bridge will cover the critical range of the spectrum turnover, which reflects the horizon scale at the time of matter-radiation equality. An example of what may be expected from the Sloan survey is shown in Figure 6; a clear determination of  $P(k)$  over a wide range of scales is expected in the near future. This will enable the determination of the initial spectrum of fluctuations at recombination that gave rise to the structure we see today and will shed light on the cosmological model parameters that may be responsible for that spectrum (such as  $\Omega_m h$  and the nature of the dark matter). In the next decade,  $P(k)$  will also be determined from the MBR anisotropy measurements on small scales ( $\sim 0.1^\circ$  to  $\sim 5^\circ$ ) [see P. Steinhardt’s contribution in these proceedings], allowing a most important overlap in the determination of the galaxy  $P(k)$  from redshift surveys and the mass  $P(k)$  from the MBR anisotropy. These data will place constraints on cosmological parameters including  $\Omega (= \Omega_m + \Omega_\Lambda), \Omega_m, \Omega_b, h$ , and the nature of the dark matter itself.

## 2.2. Clusters and Large-Scale Structure

The correlation function of clusters of galaxies efficiently quantifies the large-scale structure of the universe. Clusters are correlated in space more strongly than are individual galaxies, by an order of magnitude, and their correlation extends to considerably larger scales ( $\sim 50h^{-1}$  Mpc). The cluster correlation strength increases with richness ( $\propto$  luminosity or mass) of the system from single galaxies to the richest clusters 10, 2. Here “richness” refers to the number of cluster galaxies within a given linear radius of the cluster center and within a given luminosity range (e.g., 1). The correlation strength also increases with the mean spatial separation of the clusters 53, 4. This dependence results in a “universal” dimensionless cluster correlation function; the cluster dimensionless correlation scale is

constant for all clusters when normalized by the mean cluster separation.

Empirically, two general relations have been found 12 for the correlation function of clusters of galaxies,  $\xi_i = A_i r^{-1.8}$ :

$$A_i \propto N_i , \tag{2}$$

$$A_i \simeq (0.4d_i)^{1.8} , \tag{3}$$

where  $A_i$  is the amplitude of the cluster correlation function,  $N_i$  is the richness of the galaxy clusters of type  $i$ , and  $d_i$  is the mean separation of the clusters. Here  $d_i = n_i^{-1/3}$ , where  $n_i$  is the mean spatial number density of clusters of richness  $N_i$  in a volume-limited, richness-limited complete sample. The first relation, equation (2), states that the amplitude of the cluster correlation function increases with cluster richness, i.e., rich clusters are more strongly correlated than poorer clusters. The second relation, equation (3), states that the amplitude of the cluster correlation function depends on the mean separation of clusters (or, equivalently, on their number density); the rarer, large mean separation richer clusters are more strongly correlated than the more numerous poorer clusters. Equations (2) and (3) relate to each other through the richness function of clusters, i.e., the number density of clusters as a function of their richness. Equation (3) describes a universal scale-invariant (dimensionless) correlation function with a correlation scale  $r_{o,i} = A_i^{1/1.8} \simeq 0.4d_i$  (for  $30 \lesssim d_i \lesssim 90h^{-1}$  Mpc).

There are some conflicting statements in the literature about the precise values of the correlation amplitude,  $A_i$ . Nearly all these contradictions are caused by not taking account of equation (2). When apples are compared to oranges, or the clustering of rich clusters is compared to the clustering of poorer clusters, differences are expected and observed.

Figure 7 clarifies the observational situation. The  $A_i(d_i)$  relation for groups and clusters of various richnesses is presented in the figure. The recent automated cluster surveys of APM 20 and EDCC 40 are consistent with the predictions of equations (2) and (3), as is the correlation function of X-ray selected ROSAT clusters of galaxies 47, 7. Bahcall and Cen 7 show that a flux-limited sample of X-ray selected clusters will exhibit a correlation scale that is smaller than that of a volume-limited, richness-limited sample of comparable apparent spatial density since the flux-limited sample contains poor groups nearby and only the richest clusters farther away. Using the richness-dependent cluster correlations of equations (2) and (3), Bahcall and Cen 7 find excellent agreement with the observed flux-limited X-ray cluster correlations of Romer et al. 47. Comparison of the observed cluster correlation function with cosmological models strongly constrains the model parameters (see below).

The observed mass function (MF),  $n(> M)$ , of clusters of galaxies, which describes the number density of clusters above a threshold mass  $M$ , can be used as a critical test

of theories of structure formation in the universe. The richest, most massive clusters are thought to form from rare high peaks in the initial mass-density fluctuations; poorer clusters and groups form from smaller, more common fluctuations. Bahcall and Cen 6 determined the MF of clusters of galaxies using both optical and X-ray observations of clusters. Their MF is presented in Figure 8. The function is well fit by the analytic expression

$$n(> M) = 4 \times 10^{-5} (M/M^*)^{-1} \exp(-M/M^*) h^3 \text{ Mpc}^{-3} , \quad (4)$$

with  $M^* = (1.8 \pm 0.3) \times 10^{14} h^{-1} M_\odot$ , (where the mass  $M$  represents the cluster mass within  $1.5h^{-1}$  Mpc radius).

Bahcall and Cen 5 compared the observed mass function and correlation function of galaxy clusters with predictions of N-body cosmological simulations of standard ( $\Omega_m = 1$ ) and nonstandard ( $\Omega_m < 1$ ) CDM models. They find that none of the standard  $\Omega_m = 1$  CDM models, with any normalization, can reproduce both the observed correlation function and the mass function of clusters. A low-density ( $\Omega_m \sim 0.2\text{--}0.3$ ) CDM-type model, however, provides a good fit to both sets of observations (see Figs. 8–11). The constraints on  $\Omega_m$  are model dependent; a mixed hot + cold dark matter model, for example, with  $\Omega_m = 1$ , is also consistent with the cluster data.

The observed cluster mass function is presented in Figure 8 together with the results of CDM simulations. The standard CDM model ( $\Omega_m = 1$ ) is presented for several bias parameters  $b$  [where  $b$  represents the overdensity of galaxies relative to the mass overdensity; see § 2.1]; only the unbiased case,  $b \sim 1$ , is consistent with the COBE results. This unbiased model, however, is excluded by the observed mass function: it predicts a much larger number of rich clusters than is observed. The larger bias model of  $b \sim 2$ , while providing a more appropriate mean abundance of rich clusters, is too steep for the observed mass function; it is also incompatible with the COBE results.

The low-density, low-bias CDM model, with  $\Omega_m \approx 0.25$  and  $b \approx 1$ , (with or without  $\Lambda$ ) is consistent with the observed mass function (Fig. 8).

How does the CDM model agree with the observations of cluster correlations? Bahcall and Cen 5 used the N-body ( $N \sim 10^7$ ) simulations to determine the model cluster correlation function as a function of cluster mean separations  $d$ . The CDM results for clusters corresponding to the rich Abell clusters (richness class  $R \geq 1$ ) with  $d = 55h^{-1}$  Mpc are presented in Figure 9 together with the observed correlations 10, 43. The results indicate that the standard  $\Omega_m = 1$  CDM models are inconsistent with the observations; they cannot provide either the strong amplitude or the large scales ( $\gtrsim 50h^{-1}$  Mpc) to which the cluster correlations are observed. Similar results are found for the APM and EDCC clusters.

The low-density, low-bias model is consistent with the observed cluster correlation function. It reproduces both the strong amplitude and the large scale to which the cluster correlations are detected. Such a model is the only scale-invariant CDM model that is consistent with both cluster correlations and the cluster mass function.

The dependence of the observed cluster correlation on  $d$  was tested in the simulations (5). The results are shown in Figure 10 for the low-density model. The dependence of correlation amplitude on mean separation is clearly seen in the simulations. To compare this result directly with observations, we plot in Figure 11 the dependence of the correlation scale,  $r_o$ , on  $d$  for both the simulations and the observations. The low-density model agrees well with the observations, yielding  $r_o \approx 0.4d$ , as observed. The  $\Omega_m = 1$  model, while also showing an increase of  $r_o$  with  $d$ , yields considerably smaller correlation scales and a much slower increase of  $r_o(d)$ .

What causes the observed dependence on cluster richness [Eqs. (2–3)]? The dependence, seen both in the observations and in the simulations, is most likely caused by the statistics of rare peak events, which Kaiser 33 suggested as an explanation of the observed strong increase of correlation amplitude from galaxies to rich clusters. The correlation function of rare peaks in a Gaussian field increases with their selection threshold. Since more massive clusters correspond to a higher threshold, implying rarer events and thus larger mean separation, equation (3) results. A fractal distribution of galaxies and clusters would also produce equation (3) (e.g., 53).

### 3. Peculiar Motions on Large Scales

How is the mass distributed in the universe? Does it follow, on the average, the light distribution? To address this important question, peculiar motions on large scales are studied in order to directly trace the mass distribution. It is believed that the peculiar motions (motions relative to a pure Hubble expansion) are caused by the growth of cosmic structures due to gravity [see the presentations by Ostriker, Peebles, and Steinhardt]. A comparison of the mass-density distribution, as reconstructed from peculiar velocity data, with the light distribution (i.e., galaxies) provides information on how well the mass traces light 21, 52. The basic underlying relation between peculiar velocity and density is given by

$$\vec{\nabla} \cdot \vec{v} = -\Omega_m^{0.6} \delta_m = -\Omega_m^{0.6} \delta_g / b \quad (5)$$

where  $\delta_m \equiv (\Delta\rho/\rho)_m$  is the mass overdensity,  $\delta_g$  is the galaxy overdensity, and  $b \equiv \delta_g/\delta_m$  is the bias parameter discussed in § 2. A formal analysis yields a measure of the parameter  $\beta \equiv \Omega_m^{0.6}/b$ . Other methods that place constraints on  $\beta$  include the anisotropy in the galaxy

distribution in the redshift direction due to peculiar motions (see 52 for a review).

Measuring peculiar motions is difficult. The motions are usually inferred with the aid of measured distances to galaxies or clusters that are obtained using some (moderately-reliable) distance-indicators (such as the Tully-Fisher or  $D_n - \sigma$  relations), and the measured galaxy redshift. The peculiar velocity  $v_p$  is then determined from the difference between the measured redshift velocity,  $cz$ , and the measured Hubble velocity,  $v_H$ , of the system (the latter obtained from the distance-indicator):  $v_p = cz - v_H$ .

A comparison between the density distribution of IRAS galaxies and the mass-density distribution reconstructed from the observed peculiar motions of galaxies in the supergalactic plane is presented in Figure 12 21, 52. The distribution of mass and light in this case appear to be similar.

A summary of all measurements of  $\beta$  made so far is presented in Figure 13 52. The dispersion in the current measurements of  $\beta$  is very large; the various determinations range from  $\beta \sim 0.4$  to  $\sim 1$ , implying, for  $b \simeq 1$ ,  $\Omega_m \sim 0.2$  to  $\sim 1$ . No strong conclusion can therefore be reached at present regarding the values of  $\beta$  or  $\Omega_m$ . The larger and more accurate surveys currently underway, including high precision velocity measurements, may lead to the determination of  $\beta$  and possibly its decomposition into  $\Omega_m$  and  $b$  (e.g., 18).

Clusters of galaxies can also serve as efficient tracers of the large-scale peculiar velocity field in the universe 8. Measurements of cluster peculiar velocities are likely to be more accurate than measurements of individual galaxies, since cluster distances can be determined by averaging a large number of cluster members as well as by using different distance indicators. Using large-scale cosmological simulations, Bahcall et al. 8 find that clusters move reasonably fast in all the cosmological models studied, tracing well the underlying matter velocity field on large scales. The clusters exhibit a Maxwellian distribution of peculiar velocities as expected from Gaussian initial density fluctuations. The model cluster 3-D velocity distribution, presented in Figure 14, typically peaks at  $v \sim 600 \text{ km s}^{-1}$  and extends to high cluster velocities of  $\sim 2000 \text{ km s}^{-1}$ . The low-density CDM model exhibits somewhat lower velocities (Fig. 14). Approximately 10% of all model rich clusters (1% for low-density CDM) move with  $v \gtrsim 10^3 \text{ km s}^{-1}$ . A comparison of model expectation with the available data of cluster velocities is presented in Figure 15 8. The cluster velocity data are not sufficiently accurate at present to place constraints on the models; however, improved cluster velocities, expected in the next several years, should help constrain the cosmology.

Cen, Bahcall and Gramann 15 have recently determined the velocity correlation function of clusters in different cosmologies. They find that close cluster pairs, with separations  $r \lesssim 10h^{-1} \text{ Mpc}$ , exhibit strong attractive motions; the pairwise velocities depend sensitively

on the model. The mean pairwise attractive cluster velocities on  $5h^{-1}$  Mpc scale ranges from  $\sim 1700 \text{ km s}^{-1}$  for  $\Omega_m = 1$  CDM to  $\sim 700 \text{ km s}^{-1}$  for  $\Omega_m = 0.3$  CDM 15. The cluster velocity correlation function, presented in Figure 16, is negative on small scales—indicating large attractive velocities, and is positive on large scales, to  $\sim 200h^{-1}$  Mpc—indicating significant bulk motions in the models. None of the models reproduce the very large bulk flow of clusters on  $150h^{-1}$  Mpc scale,  $v \simeq 689 \pm 178 \text{ km s}^{-1}$ , recently reported by Lauer and Postman 37. The bulk flow expected on this large scale is generally  $\lesssim 200 \text{ km s}^{-1}$  for all the models studied ( $\Omega_m = 1$  and  $\Omega_m \simeq 0.3$  CDM, and PBI; 15, 51).

#### 4. Dark Matter and Baryons in Clusters of Galaxies

The gravitational potential of clusters of galaxies has traditionally been studied with the aid of the observed velocity dispersion of the cluster galaxies and the virial theorem (e.g. 62, 44). The cluster potential can also be estimated by the temperature of the hot intracluster gas as determined from X-ray observations (e.g., 32, 48) and by the weak gravitational lens distortion of background galaxies caused by the intervening cluster mass 55, 34. Sufficient data are now available from optical observations (galaxy velocity dispersion in clusters), X-ray observations (the temperature of the intracluster gas), and initial estimates from gravitational lensing, so that the results can be intercompared. The cluster mass determinations are, on the average, consistent with each other 3.

The optical and X-ray observations of rich clusters of galaxies yield cluster masses that range from  $\sim 10^{14}$  to  $\sim 10^{15}h^{-1}M_\odot$  within  $1.5h^{-1}$  Mpc radius of the cluster center. When normalized by the cluster luminosity, a median value of  $M/L_B \simeq 300h$  is observed for rich clusters. This mass-to-light ratio implies a dynamical mass density of  $\Omega_{\text{dyn}} \sim 0.2$  on  $\sim 1.5h^{-1}$  Mpc scale. If, as suggested by theoretical prejudice, the universe has critical density ( $\Omega_m = 1$ ), then most of the mass in the universe *cannot* be concentrated in clusters, groups and galaxies; the mass would have to be distributed more diffusely than the light.

A recent analysis of the mass-to-light ratio of galaxies, groups and clusters 9 suggests that while the  $M/L$  ratio of galaxies increases with scale up to radii of  $R \sim 0.1\text{--}0.2h^{-1}$  Mpc, due to the large dark halos around galaxies (see Fig. 17), this ratio appears to flatten and remain approximately constant for groups and rich clusters, to scales of  $\sim 1.5$  Mpc, and possibly even to the larger scales of superclusters (Fig. 18). The flattening occurs at  $M/L_B \simeq 200\text{--}300h$ , corresponding to  $\Omega_m \sim 0.2$ . This observation may suggest that most of the dark matter is associated with the dark halos of galaxies and that clusters do *not* contain a substantial amount of additional dark matter, other than that associated with (or torn-off from) the galaxy halos, and the hot intracluster medium. Unless the distribution of

matter is very different from the distribution of light, with large amounts of dark matter in the “voids” or on very large scales, the cluster observations suggest that the mass density in the universe may be low,  $\Omega_m \sim 0.2$  (or  $\Omega_m \sim 0.3$  for a small bias of  $b \sim 1.5$ ).

Clusters of galaxies contain many baryons. Within  $1.5h^{-1}$  Mpc of a rich cluster, the X-ray emitting gas contributes  $\sim 3\text{--}10h^{-1.5}\%$  of the cluster virial mass (or  $\sim 10\text{--}30\%$  for  $h = 1/2$ ) 14, 59. Visible stars contribute only a small additional amount to this value. Standard Big-Bang nucleosynthesis limits the mean baryon density of the universe to  $\Omega_b \sim 0.015h^{-2}$  57. This suggests that the baryon fraction in some rich clusters exceeds that of an  $\Omega_m = 1$  universe by a large factor 60, 38. Detailed hydrodynamic simulations 60, 38 suggest that baryons are not preferentially segregated into rich clusters. It is therefore suggested that either the mean density of the universe is considerably smaller, by a factor of  $\sim 3$ , than the critical density, or that the baryon density of the universe is much larger than predicted by nucleosynthesis. The observed baryonic mass fraction in rich clusters, when combined with the nucleosynthesis limit, suggests  $\Omega_m \sim 0.2\text{--}0.3$ ; this estimate is consistent with  $\Omega_{\text{dyn}} \sim 0.2$  determined from clusters.

## 5. Is $\Omega_m < 1$ ?

Much of the observational evidence from clusters and from large-scale structure suggests that the mass density of the universe is sub-critical:  $\Omega_m \sim 0.2\text{--}0.3$  (§§ 2–4). I summarize these results below:

- The masses and the  $M/L(R)$  relations of galaxies, groups, and clusters of galaxies suggest  $\Omega_m \sim 0.2\text{--}0.3$  (§ 4).
- The high baryon fraction in clusters of galaxies suggests  $\Omega_m \sim 0.2\text{--}0.3$  (§ 4).
- Various observations of large-scale structure (the mass function, the power spectrum, and the peculiar velocities on Mpc scale) all suggest  $\Omega_m h \sim 0.2$  (for a CDM-type spectrum) (§ 2).
- The frequent occurrence of evolved systems of galaxies and clusters at high redshifts ( $z \sim 1$ ) also suggest a low-density universe, in which galaxy systems form at earlier times. No quantitative measures are yet available, however; this topic will be further clarified within the next several years using observations with HST, Keck, other deep ground-based observations, and deep X-ray surveys of clusters.
- If  $H_o \sim 70\text{--}80 \text{ km s}^{-1} \text{ Mpc}^{-1}$ , as indicated by a number of recent observations (25 and references therein), then the observed age of the oldest stars requires  $\Omega_m \ll 1$ .

- Peculiar motions on large scales are too uncertain at the present time (suggesting density values that range from  $\Omega_m \sim 0.2$  to  $\sim 1$ ) to shed much light on  $\Omega_m$ . Future results, based on larger and more accurate surveys, will help constrain this parameter (§ 3).

## 6. The SDSS and Large-Scale Structure

I will now describe the general characteristics of the Sloan Digital Sky Survey (SDSS) (in Section 6.1) and then tell you (in Section 6.2) some of the exciting things we expect to do with this survey using clusters of galaxies, my own favorite. You should know that my choice of topics reflects primarily my own research activity and that the SDSS will do many extraordinary and important things with individual galaxies, quasars, and stars.

### 6.1. *The Sloan Digital Sky Survey*

Large surveys, especially in three dimensions, are vital for the study of clustering and large-scale structure of the universe. The surveys must cover huge volumes in order to investigate the largest-scale structure. They can provide accurate, systematic, and complete data bases of galaxies, clusters, superclusters, voids, and quasars, which can be used to study the universal structure and its cosmological implications. The surveys will allow both broad statistical studies of large samples as well as specific detailed studies of individual systems.

In this section, I summarize some of the fundamental contributions that large-scale surveys will offer for the study of clustering and large-scale structure. I will concentrate on the planned Sloan Digital Sky Survey (SDSS; 61), which is the largest survey currently planned; however most of the discussion is generally applicable to large-scale imaging and spectroscopic surveys.

The Sloan survey will make a powerful contribution to the investigation of large-scale structure because of the survey's size, uniformity, and the high quality of its photometric and spectroscopic data. These characteristics will allow galaxy clustering in the present-day universe to be measured with unprecedented precision and detail. The survey will be able to resolve some of the unsolved problems listed in § 1, as well as address questions we have not yet thought to ask. There will be a lot of problems for students to solve with these data!

The SDSS will produce a complete photometric and spectroscopic survey of half the northern sky ( $\pi$  steradians). The photometric survey will image the sky in five colors ( $u'$ ,  $g'$ ,  $r'$ ,  $i'$ ,  $z'$ ), using a large array of thirty  $2048^2$  pixel CCD chips; the imaging sur-

vey will contain nearly  $5 \times 10^7$  galaxies to  $g' \sim 23^m$ , a comparable number of stars, and about  $10^6$  quasar candidates (selected on the basis of the five colors). The imaging data will then be used to select the brightest  $\sim 10^6$  galaxies and  $\sim 10^5$  quasars for which high-resolution spectra will be obtained (to  $r' \sim 18^m$  and  $19^m$ , respectively) using 640 fibers on two high-resolution ( $R = 2000$ ) double-spectrographs. Both the imaging and spectroscopic surveys will be done on the same 2.5-meter wide-field ( $3^\circ$  FOV) special purpose telescope located at Apache Point, NM. The imaging survey will also be used to produce a catalog in five colors of all the detected objects and their main characteristic parameters. In the southern hemisphere, the SDSS will image repeatedly a long and narrow strip of the sky,  $\sim 75^\circ \times 3^\circ$ , reaching  $2^m$  fainter than the large-scale northern survey. The repeated imaging, in addition to allowing the detection of fainter images, will also be crucial for the detection of variable objects.

Figure 2 shows a simulated distribution in redshift space of galaxies expected from the Sloan Survey in a  $6^\circ$  thick slice along the survey equator. This figure, based on a cold-dark-matter cosmological model simulation, corresponds to approximately 6% of the galaxy redshift survey. The redshift histogram of galaxies in the simulated spectroscopic survey peaks at  $z \sim 0.1\text{--}0.15$ , with a long tail to  $z \sim 0.4$ .

Several thousand rich clusters of galaxies will be identified in the survey, many with a large number of measured galaxy redshifts per cluster (from the complete spectroscopic survey). Several hundred large superclusters will also be identified. This will provide at least a ten-fold increase in the number of clusters and superclusters over presently available samples.

Currently under construction, the test year for the SDSS system will begin observations in 1997. More detailed information on the SDSS project is provided in 61.

## 6.2. *Clusters of Galaxies*

Large-scale surveys such as the SDSS will provide a much needed advance in the systematic study of clusters of galaxies, which is currently limited by the unavailability of modern, accurate, complete, and objectively-selected catalogs of clusters, and by the limited photometric and redshift information for the catalogs that do exist. The SDSS will select clusters algorithmically. From the  $10^6$  galaxies in the spectroscopic sample, we can identify clusters by searching for density enhancements in redshift space. We can also identify clusters from the much larger photometric sample ( $5 \times 10^7$  galaxies) by searching for density enhancements in position-magnitude-color space. We expect to find approximately 4000 clusters of galaxies

with a redshift tail to  $z \sim 0.5$ ; many of the clusters will have a large number of measured galaxy redshifts per cluster (hundreds of redshifts for nearby clusters), and at least one or two redshifts for the more distant clusters. This complete sample of clusters can be used to investigate numerous topics in the study of clustering and large-scale structure. I briefly illustrate some of these topics below. The solutions of the problems outlined below will involve the participation of many graduate students!

### 6.2.1. *Clusters as Tracers of Large-Scale Structure*

Clusters are efficient tracers of the large-scale structure. Studies of the cluster distribution have yielded important results even though the number of cluster redshifts in complete samples has been quite small,  $\sim 100$  to 300. The SDSS will put such studies on a much firmer basis because of the increased sample size (roughly an order of magnitude more redshifts), the objective and automated identification methods, and the use of cluster-finding algorithms that are less subject to projection contamination.

Catalogs of nearby superclusters have been constructed using Abell clusters with known redshifts, revealing structures on scales as large as  $\sim 150h^{-1}$  Mpc 11. There are claims for still larger,  $\sim 300h^{-1}$  Mpc structures in the Abell cluster distribution 54; these are still controversial 46. The SDSS redshift survey will identify a considerably bigger sample of superclusters and will clarify the possible existence of structure on very large scales. The sizeable cluster sample should also clarify the relation between the cluster distribution and the galaxy distribution. Cluster peculiar velocities, obtained directly from distance indicators such as the  $D_n - \sigma$  measurements and indirectly from the anisotropy of the cluster correlation function in redshift space, will provide information about the internal dynamics of superclusters and the mass distribution on large scales.

The high amplitude of the cluster correlation function,  $\xi_{cc}(r)$ , provided early evidence for strong clustering on large scales (§ 2). The complete sample of SDSS clusters, objectively defined from uniform and accurate photometric and spectroscopic data, will allow a measurement of  $\xi_{cc}$  free from systematic effects. We can extend the correlation analysis in several ways, examining in detail the richness dependence of  $\xi_{cc}$  as well as the dependence of the cluster correlation on other cluster properties (e.g., velocity dispersion, morphology).

The alignment of galaxies with their host clusters, and of clusters with their neighboring clusters, their host superclusters, and other large-scale structures such as sheets and filaments is of great interest. While the alignment of cD galaxies with their clusters is relatively well established 13, alignments at larger scales are still uncertain 17. The SDSS will provide a

very large sample for alignment studies, including accurate position angles and inclinations. The existence of large-scale alignments may place interesting constraints on the origin of structure in various cosmological models 58.

### 6.2.2. Global Cluster Properties

The complete cluster survey will allow a detailed investigation of intrinsic cluster properties. From the 2-D and 3-D information, we will be able to determine accurately such properties as cluster richness, morphology, density and density profile, core radius, velocity dispersion profile, optical luminosity, and galaxy content, and to look for correlations between these properties. The cluster catalogs will be matched with data in other bands, in particular the X-ray. This will allow a systematic detailed study of global cluster properties and their cross-correlation.

Measurements of galaxy density, morphology, velocity dispersion, and X-ray emission will shed light on the nature of the intracluster medium and its impact on the member galaxies, and on the relative distribution of baryonic and dark matter. High surface mass density clusters will be candidates for gravitational lenses; we can search the photometric data for systematically distorted background galaxies, especially in the deeply-observed southern strip, and target these clusters for yet deeper imaging surveys with larger telescopes. These lensing studies will allow mapping out the dark matter distribution within the clusters 55, 34.

The large statistical sample of clusters will produce new insights into a number of issues associated with structure formation and evolution:

- We will be able to calculate velocity dispersions for  $\sim 1000$  clusters with  $z \lesssim 0.2$  compared to a few dozen clusters with reliable dispersion measurements currently available. For nearer clusters, we will have well-sampled galaxy density profiles and velocity dispersion profiles; these allow careful cluster mass determinations. The distributions of cluster masses and velocity dispersions, i.e., the cluster mass function and velocity function will be determined accurately.
- With optical luminosities, galaxy profiles, and velocity dispersion profiles, we can measure accurate mass-to-light ratios for a large sample of clusters. Combined with X-ray observations of clusters, the baryon fraction can be determined more accurately. These provide constraints on  $\Omega_m$  and the bias parameter of galaxies in clusters.
- The density and dispersion profiles also retain clues about the history of cluster formation. The frequency of subclustering and non-virial structures in clusters 26 tells

us whether clusters are dynamically old or young. In a gravitational instability model with  $\Omega_m = 1$ , structure continues to form today, while in a low- $\Omega$ , open universe, clustering freezes out at moderate redshift. Cluster profiles and substructure statistics thus provide a diagnostic for  $\Omega_m$ , a diagnostic which is independent of the direct measures of the mass density.

- The evolution of the cluster population provides another diagnostic for  $\Omega_m$ . Current investigations are limited by the small numbers of known high-redshift clusters, and by the fact that high- and low-redshift clusters are selected in different ways. The uniform SDSS cluster sample will greatly improve the current situation. The number of clusters will be large; we will have redshifts for brightest cluster galaxies to  $z \approx 0.5$  by extending the main redshift survey limit  $\sim 1^m$  fainter for brightest cluster galaxy candidates, and for more distant clusters we can obtain fairly accurate estimated redshifts from the photometry alone (using the colors and apparent luminosity function of member galaxies). The southern photometric survey will probe the cluster population to redshifts above unity.

### 6.2.3. Large-Scale Motions of Clusters

Peculiar motions of clusters of galaxies can be determined from the SDSS survey using distance indicators such as Tully-Fisher or  $D_n - \sigma$  for cluster galaxies, the cluster luminosity function, or the Brightest-Cluster-Member indicator. This will allow a determination of the large-scale peculiar motion of clusters to hundreds of Mpc.

## 7. Summary

Observations of large-scale structure provide a powerful tool for determining the structure of our universe, for understanding galaxy and structure formation, and for constraining cosmological models. While extraordinary progress has been made over the last decade, many important unsolved problems remain. The large observational surveys currently underway provide a way of resolving some of these questions [see also the contribution by P. Steinhardt, these proceedings]. The interested student has a great opportunity to participate in fundamental discoveries.

What problems can we expect to solve in the next decade? I believe that the large redshift surveys of galaxies, clusters of galaxies, and quasars will provide a quantitative description of structure on a wide range of scales, from  $\sim 1$  to  $\sim 10^3 h^{-1}$  Mpc, includ-

ing the determinations of the power spectrum, the correlation function, the topology, and other improved statistics (§§ 2,6). The dependence of these statistical measures on galaxy type, luminosity, surface brightness, and system type (galaxies, clusters, quasars) will also be determined and used to constrain cosmological models of galaxy formation. Accurate measurements on large scales of the peculiar motions of galaxies and clusters, and the mass distribution on large scales may take longer. Detailed X-ray surveys of galaxy clusters, combined with the large redshift and lensing surveys, will be able to resolve the problem of the baryon fraction in clusters and test suggested explanations (§ 4). Deep optical and X-ray surveys, using HST, Keck, ROSAT, ASCA, AXAF, SIRTf, plus new microwave background studies, and other deep ground-based and space-based observations, should allow a considerable increase in our understanding of the time evolution of galaxies, clusters of galaxies, quasars, and large-scale structure. Since the computed evolution of galaxy systems depends strongly on the assumed cosmology and especially on the mass density, with low-density models evolving at much earlier times than high density models, observations of the kind described here will provide some of the most critical clues needed to constrain the cosmological model over the next decade (§§ 5,6).

The quantitative description of large-scale structure and its evolution, when compared with state-of-the-art cosmological simulations to be available in the next decade (e.g. J. P. Ostriker, these proceedings), will enhance our chances of determining the cosmology of our universe. Will this goal be reached within the next decade? We will have to meet again in a decade and see.

### Acknowledgments

It is a pleasure to thank J. N. Bahcall, D. Eisenstein, K. Fisher, J. P. Ostriker, P. J. E. Peebles, H. Rood, D. Spergel, and M. Strauss for stimulating discussions and helpful comments on the manuscript. The work by N. Bahcall and collaborators is supported by NSF grant AST93-15368 and NASA graduate training grant NGT-51295.

### Bibliographic Notes

- **Bahcall, N. A. 1988, *ARA&A*, 26, 631.** A detailed review of the large-scale structure of the universe as traced with clusters of galaxies.
- **Bahcall, N. A., & Soneira, R. M. 1983, *ApJ*, 270, 20.** The first determination of the three-dimensional cluster correlation function and the richness dependence of

the cluster correlations.

- **Geller, M., & Huchra, J. 1989, *Science*, 246, 897.** A clear and exciting summary of the large-scale structure observed in the CFA redshift survey.
- **Maddox, S., Efstathiou, G., Sutherland, W., & Loveday, J. 1990, *MNRAS*, 242, 43p.** A recent determination of the angular correlation function of galaxies using the APM survey.
- **Peebles, P. J. E. 1980, *The Large-Scale Structure of the Universe*; 1993, *Principles of Physical Cosmology* (Princeton: Princeton University Press).** The standard monographs from which students (and professors) have learned the subjects of large-scale structure and cosmology.
- **Strauss, M., & Willick, J. 1995, *Physics Reports*, 261, 271.** A comprehensive review of the density and peculiar velocity fields of nearby galaxies.
- **York, D., Gunn, J. E., Kron, R., Bahcall, N. A., Bahcall, J. N., Feldman, P. D., Kent, S. M., Knapp, G. R., Schneider, D., & Szalay, A. 1993, *A Digital Sky Survey of the Northern Galactic Cap*, NSF proposal.** A detailed summary of the planned Sloan Digital Sky Survey.

## REFERENCES

Abell, G. O. 1958, *ApJS*, 3, 211.

Bahcall, N. A. 1988, *ARA&A*, 26, 631.

Bahcall, N. A. 1995, in *AIP Conference Proceedings 336, Dark Matter*, eds. S. S. Holt, & C. L. Bennett (New York: AIP), p. 201.

Bahcall, N. A., & Burgett, W. S. 1986, *ApJ*, 300, L35.

Bahcall, N. A., & Cen, R. Y. 1992, *ApJ*, 398, L81.

Bahcall, N. A., & Cen, R. Y. 1993, *ApJ*, 407, L49.

Bahcall, N. A., & Cen, R. Y. 1994, *ApJ*, 426, L15.

Bahcall, N. A., Gramann, M., & Cen, R. 1994, *ApJ*, 436, 23.

Bahcall, N. A., Lubin, L., & Dorman, V. 1995, *ApJ*, 447, L81.

- Bahcall, N. A., & Soneira, R. M. 1983, *ApJ*, 270, 20.
- Bahcall, N. A., & Soneira, R. M. 1984, *ApJ*, 277, 27.
- Bahcall, N. A., & West, M. L. 1992, *ApJ*, 392, 419.
- Binggeli, B. 1982, *A&A*, 107, 338.
- Briel, U. G., Henry, J. P., & Boringer, H. 1992, *A&A*, 259, L31.
- Cen, R., Bahcall, N. A., & Gramann, M. 1994, *ApJ*, 437, L51.
- Chincarini, G., Rood, H. J., & Thompson, L. A. 1981, *ApJ*, 249, L47.
- Chincarini, G., Vettolani, G., & de Souza, R. 1988, *A&A*, 193, 47.
- Cole, S., Fisher, K. B., & Weinberg, D. H. 1994, *MNRAS*, 267, 785.
- da Costa, L. N., et al. 1988, *ApJ*, 327, 544.
- Dalton, G., Efstathiou, G., Maddox, S., & Sutherland, W. 1992, *ApJ*, 390, L1.
- Dekel, A. 1994, *ARA&A*, 32, 371.
- de Lapparent, V., Geller, M., & Huchra, J. 1986, *ApJ*, 302, L1.
- Efstathiou, G., Sutherland, W., & Maddox, S. 1990, *Nature*, 348, 705.
- Fisher, K. B., Davis, M., Strauss, M. A., Yahil, A., & Huchra, J. P. 1993, *ApJ*, 402, 42.
- Freedman, W., et al. 1994, *Nature*, 371, 757.
- Geller, M. 1990, in *Space Telescope Symposium Series #4, Clusters of Galaxies*, eds. W. Oegerle, M. Fitchett, & L. Danly (Cambridge: Cambridge University Press).
- Geller, M., & Huchra, J. 1989, *Science*, 246, 897.
- Giovanelli, R., Haynes, M., & Chincarini, G. 1986, *ApJ*, 300, 77.
- Gregory, S. A., & Thompson, L. A. 1978, *ApJ*, 222, 784.
- Gregory, S. A., Thompson, L. A., & Tifft, W. 1981, *ApJ*, 243, 411.
- Groth, E., & Peebles, P. J. E. 1977, *ApJ*, 217, 385.
- Jones, C., & Forman, W. 1984, *ApJ*, 276, 38.

- Kaiser, N. 1984, *ApJ*, 284, L9.
- Kaiser, N., & Squires, G. 1993, *ApJ*, 404, 441.
- Kirshner, R., Oemler, A., Schechter, P., & Shectman, S. 1995, preprint (to be published in *ApJ*).
- Landy, S. D., Shectman, S. A., Lin, H., Kirshner, R. P., Oemler, A. A., & Tucker, D. 1996, *ApJ*, 456, L1.
- Lauer, T., & Postman, M. 1994, *ApJ*, 425, 418.
- Lubin, L., Cen, R., Bahcall, N. A., & Ostriker, J. P. 1996, *ApJ*, 460, 10.
- Maddox, S., Efstathiou, G., Sutherland, W., & Loveday, J. 1990, *MNRAS*, 242, 43p.
- Nichol, R., Collins, C., Guzzo, L., & Lumsden, S. 1992, *MNRAS*, 255, 21.
- Park, C., Vogele, M. S., Geller, M. J., & Huchra, J. P. 1994, *ApJ*, 431, 569.
- Peacock, J., & Dodds, S. J. 1994, *MNRAS*, 267, 1020.
- Peacock, J., & West, M. 1992, *MNRAS*, 259, 494.
- Peebles, P. J. E. 1980, *The Large-Scale Structure of the Universe* (Princeton: Princeton University Press).
- Peebles, P. J. E. 1993, *Principles of Physical Cosmology*, (Princeton University Press: Princeton).
- Postman, M., Spergel, D. N., Sutin, B., & Juskiewicz, R. 1989, *ApJ*, 346, 588.
- Romer, A.K., Collins, C., Böhringer, H., Cruddace, R., Ebeling, H., MacGillivray, H., & Voges, W. 1994, *Nature*, 372, 75.
- Sarazin, C. L. 1986, *Rev. Mod. Phys.*, 58, 1.
- Shapley, H. 1930, *Harvard Obs. Bull. No. 874*, 9.
- Smoot, G. R., Bennett, C. L., Kogut, A., Wright, E. L., Aymon, J., Boggess, N. W., Cheng, E. S., De Amici, G., Guzik, S., & Hauser, M. G. 1992, *ApJ*, 396, L1.
- Strauss, M., Cen, R., Ostriker, J. P., Postman, M., & Lauer, T. 1995, *ApJ*, 444, 507.
- Strauss, M., & Willick J. 1995, *Physics Reports*, 261, 271.

- Szalay, A., & Schramm, D. 1985, *Nature*, 314, 718.
- Tully, R. B. 1987, *ApJ*, 323, 1.
- Tyson, J. A., Wenk, R. A., & Valdes, F. 1990, *ApJ*, 349, L1.
- Vogele, M. S., Park, C., Geller, M. J., & Huchra, J. P. 1992, *ApJ*, 391, L5.
- Walker, T. P., Steigman, G., Schramm, D. N., Olive, K. A., & Kang, H. S. 1991, *ApJ*, 376, 51.
- West, M. J., Oemler, A., & Dekel, A. 1989, *ApJ*, 346, 539.
- White, D., & Fabian, A. 1995, *MNRAS*, 273, 72.
- White, S. D. M., Navarro, J. F., Evrard, A., & Frenk, C.S. 1993, *Nature*, 366, 429.
- York, D., Gunn, J. E., Kron, R., Bahcall, N. A., Bahcall, J. N., Feldman, P. D., Kent, S. M., Knapp, G. R., Schneider, D., & Szalay, A. 1993, A Digital Sky Survey of the Northern Galactic Cap, NSF proposal.
- Zwicky, F. 1957, *Morphological Astronomy* (Berlin: Springer-Verlag).

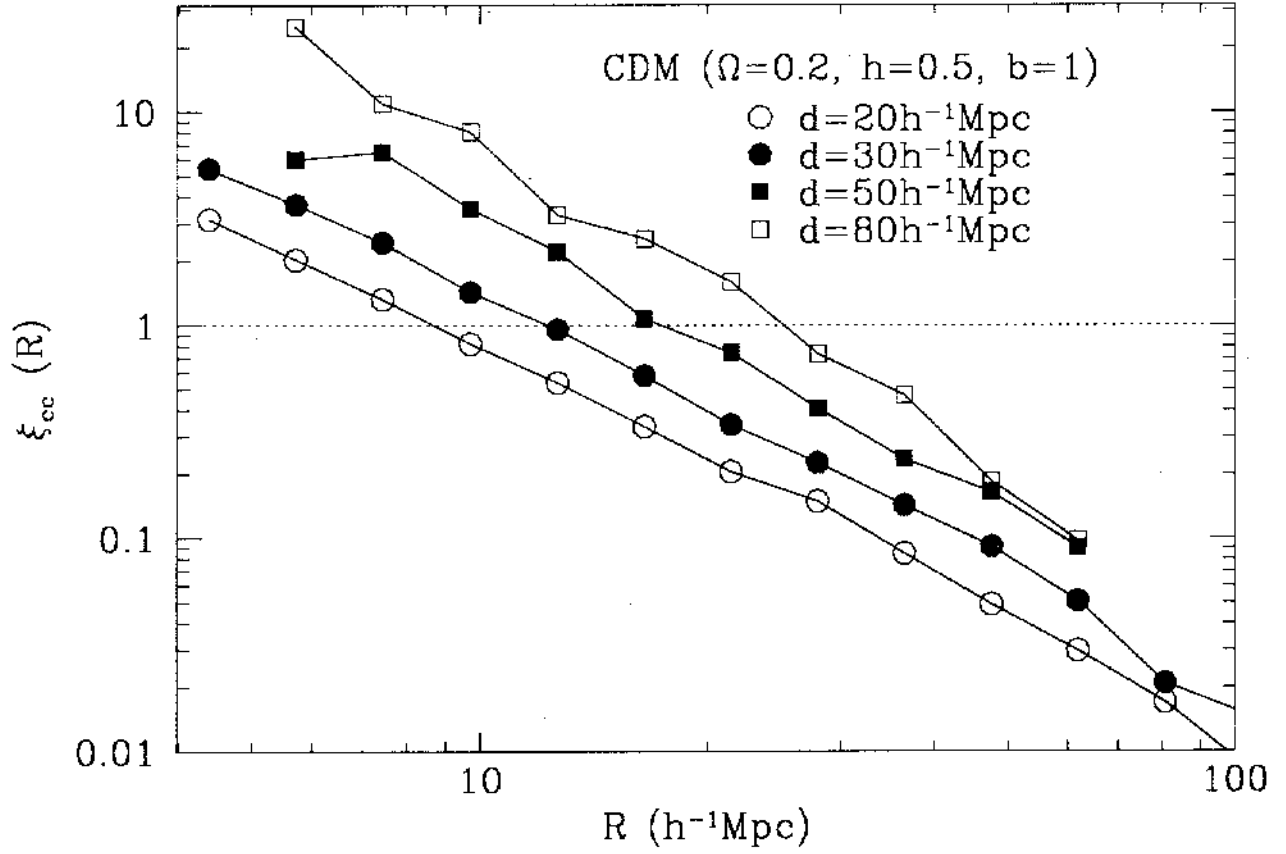


Fig. 1.— Redshift cone diagram for galaxies in the Las Campanas survey 35.

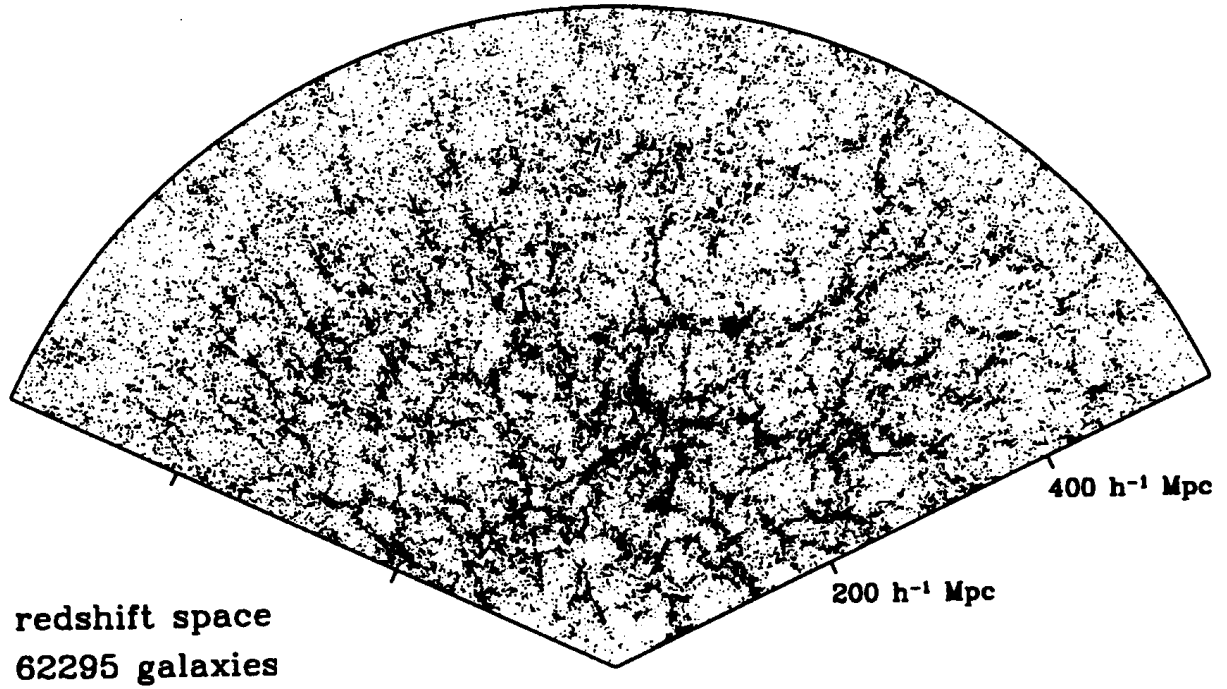


Fig. 2.— The redshift-space distribution of galaxies in a  $6^\circ$  thick slice along the SDSS survey equator from a large N-body cosmological simulation (cold-dark-matter with  $\Omega_m h \simeq 0.24$ ; Gott, et al., in preparation). This slice contains approximately 6% of the  $10^6$  galaxies in the spectroscopic survey.

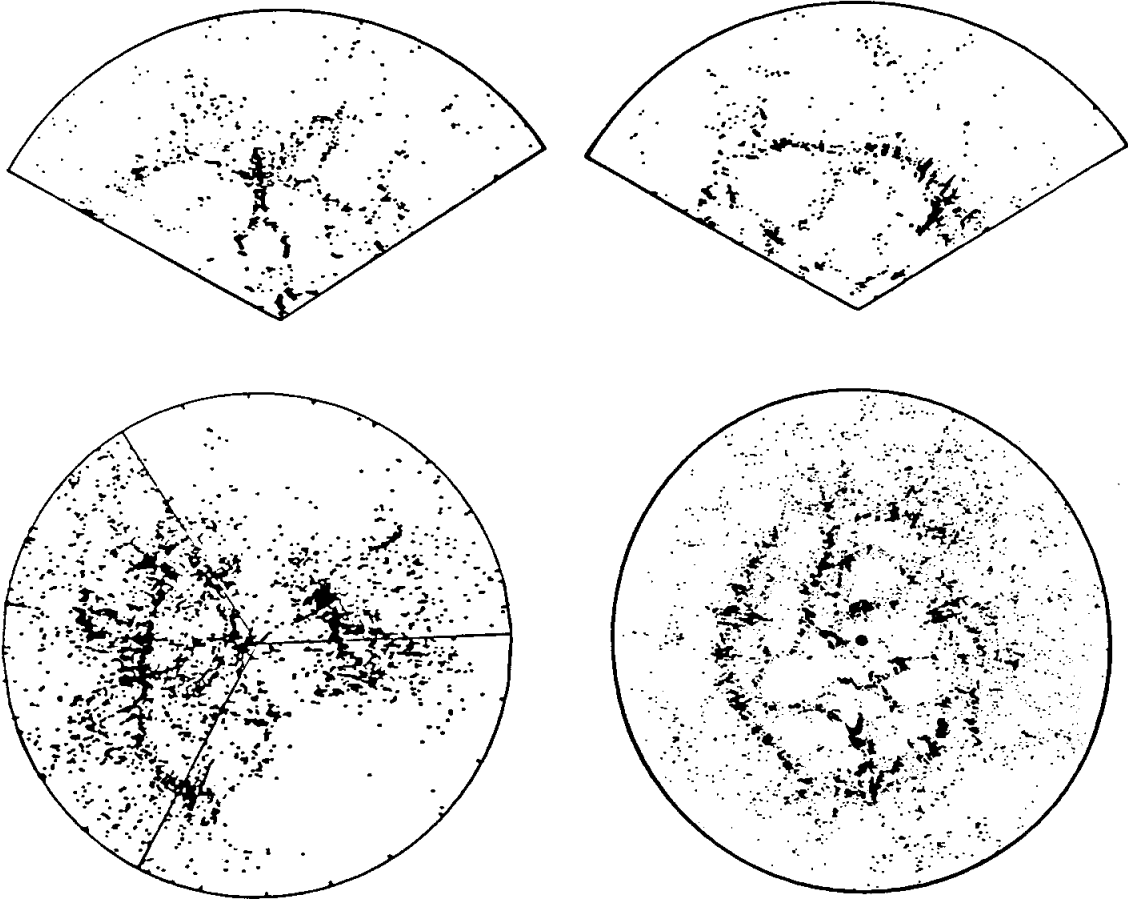


Fig. 3.— Redshift cone diagrams for observed (CfA survey) and simulated (CDM cosmology with  $\Omega_m h = 0.3$ ) galaxy (mass) distributions in the present universe. Which are data and which are simulations? The similarity of the two indicates the underlying success of basic cosmology in reproducing the observed structure.

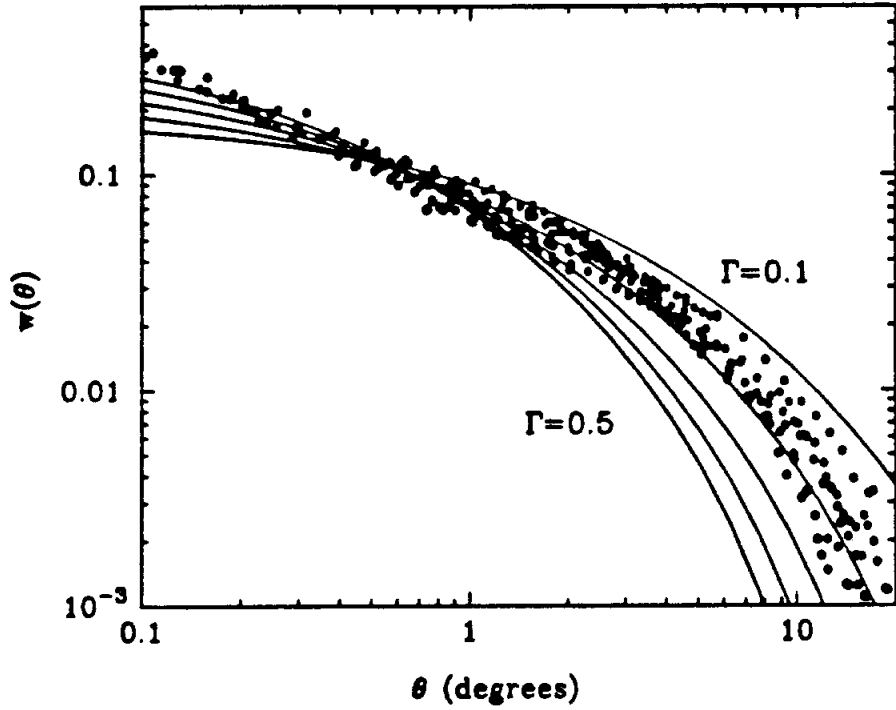


Fig. 4.— The scaled angular correlation function of galaxies measured from the APM survey plotted against linear theory predictions for CDM models (normalized to  $\sigma_8 = 1$  on  $8h^{-1}$  Mpc scale) with  $\Gamma \equiv \Omega_m h = 0.5, 0.4, 0.3, 0.2$  and  $0.1$  23.

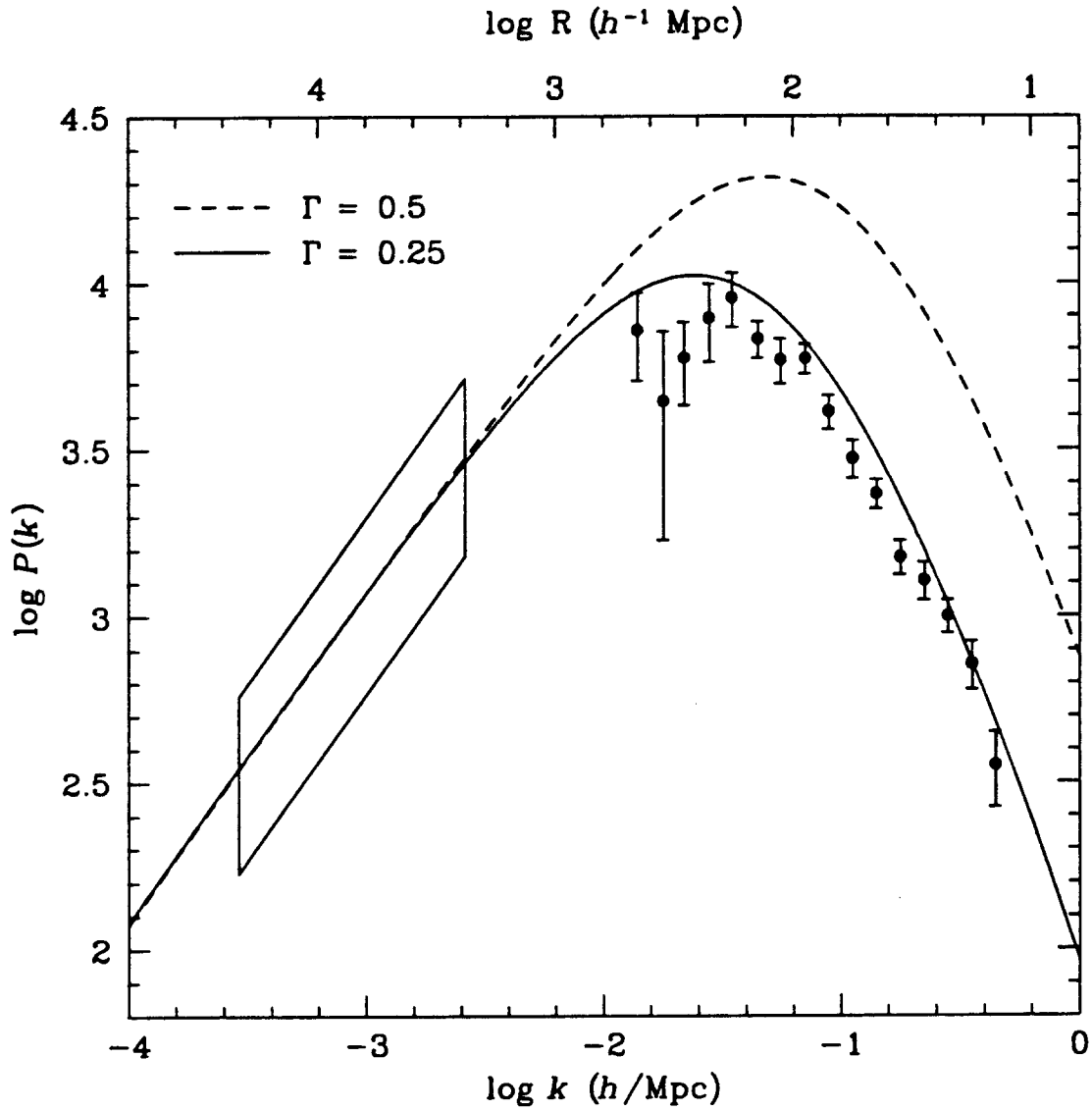


Fig. 5.— The power spectrum as derived from a variety of tracers and redshift surveys, after correction for non-linear effects, redshift distortions, and relative biases; from 42. The two curves show the Standard CDM power spectrum ( $\Gamma = 0.5$ ), and that of CDM with  $\Gamma = 0.25$ . Both are normalized to the COBE fluctuations, shown as the box on the left-hand side of the figure.

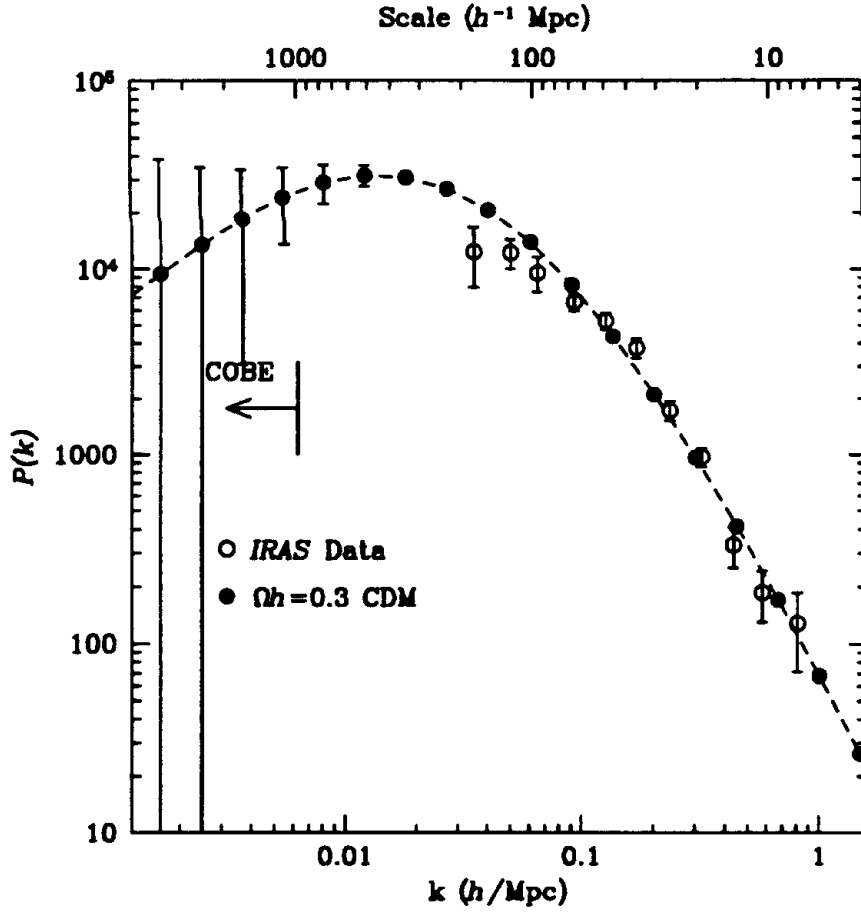


Fig. 6.— Estimate of the galaxy power spectrum that can be obtained with the Sloan Survey. The solid points and dashed line show the linear theory power spectrum of  $\Omega_m h = 0.3$  CDM, with error bar estimates appropriate for the Sloan Survey. Open points are from 24. The scales probed by COBE are shown.

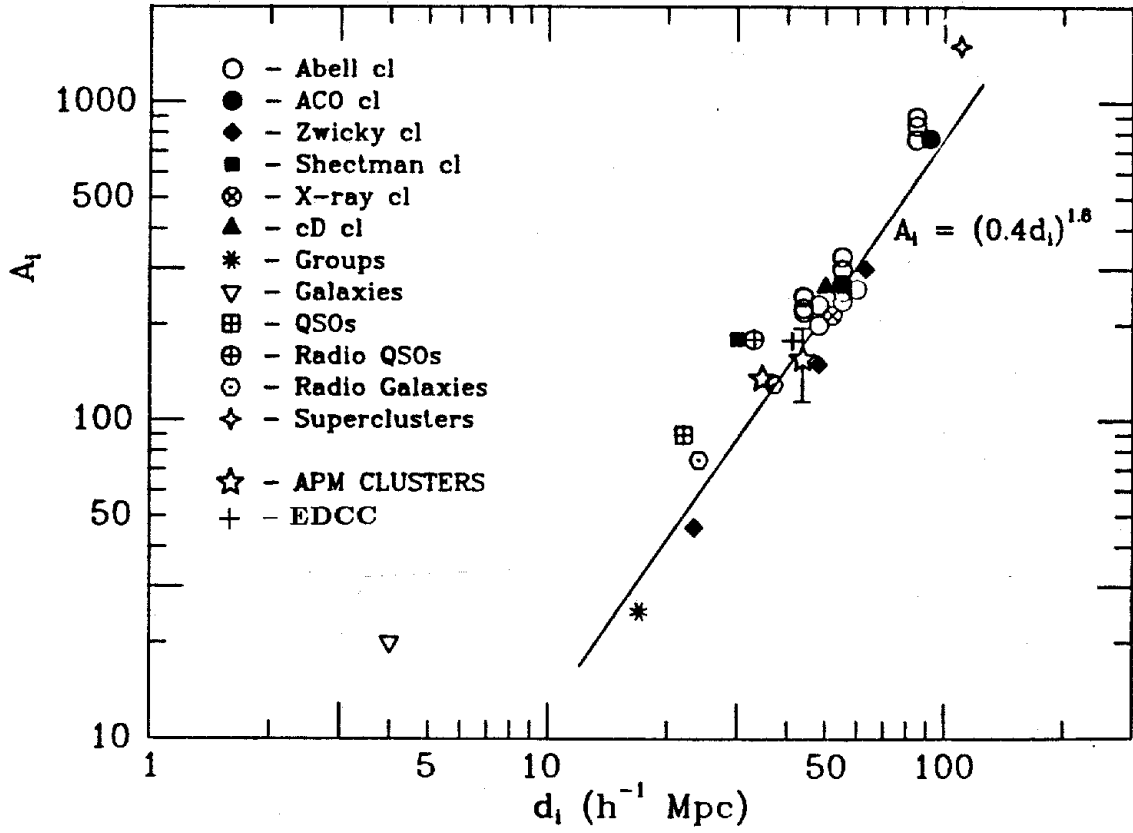


Fig. 7.— The dependence of the cluster correlation amplitude on mean cluster separation  
12.

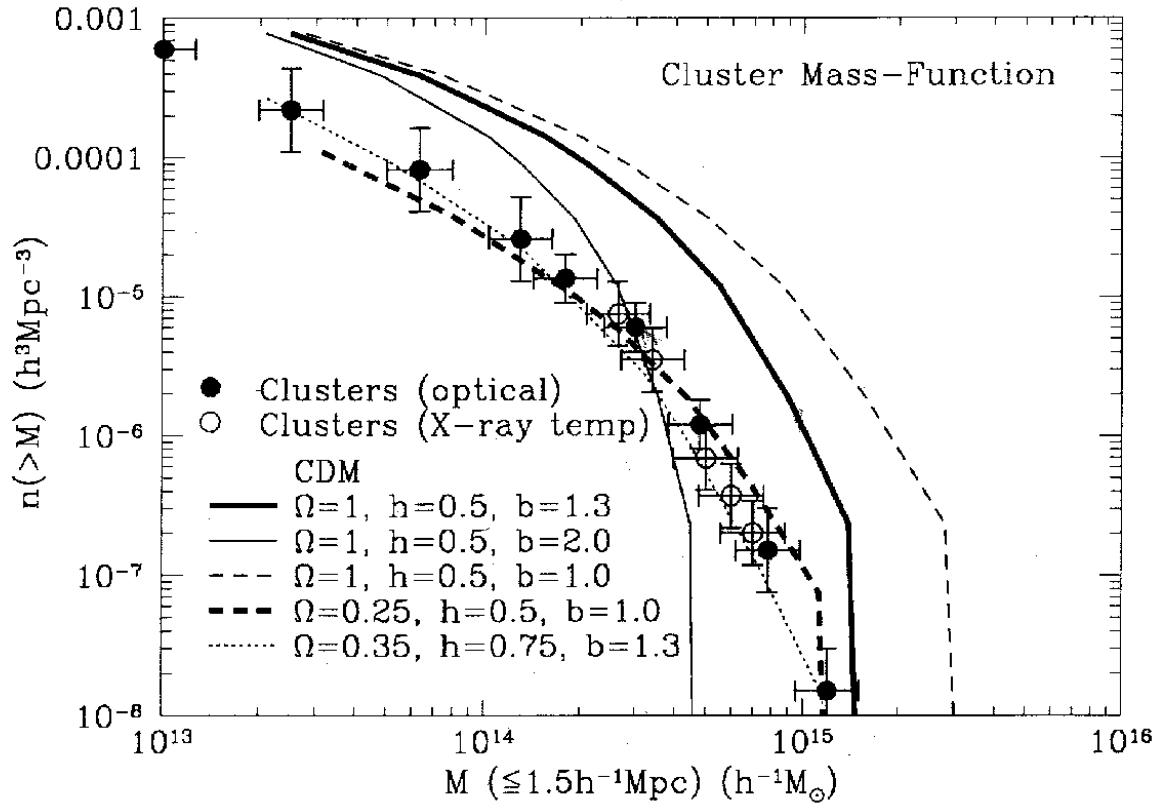


Fig. 8.— The mass function of clusters of galaxies from observations (points) and cosmological simulations of different  $\Omega_m h$  CDM models 5, 6.

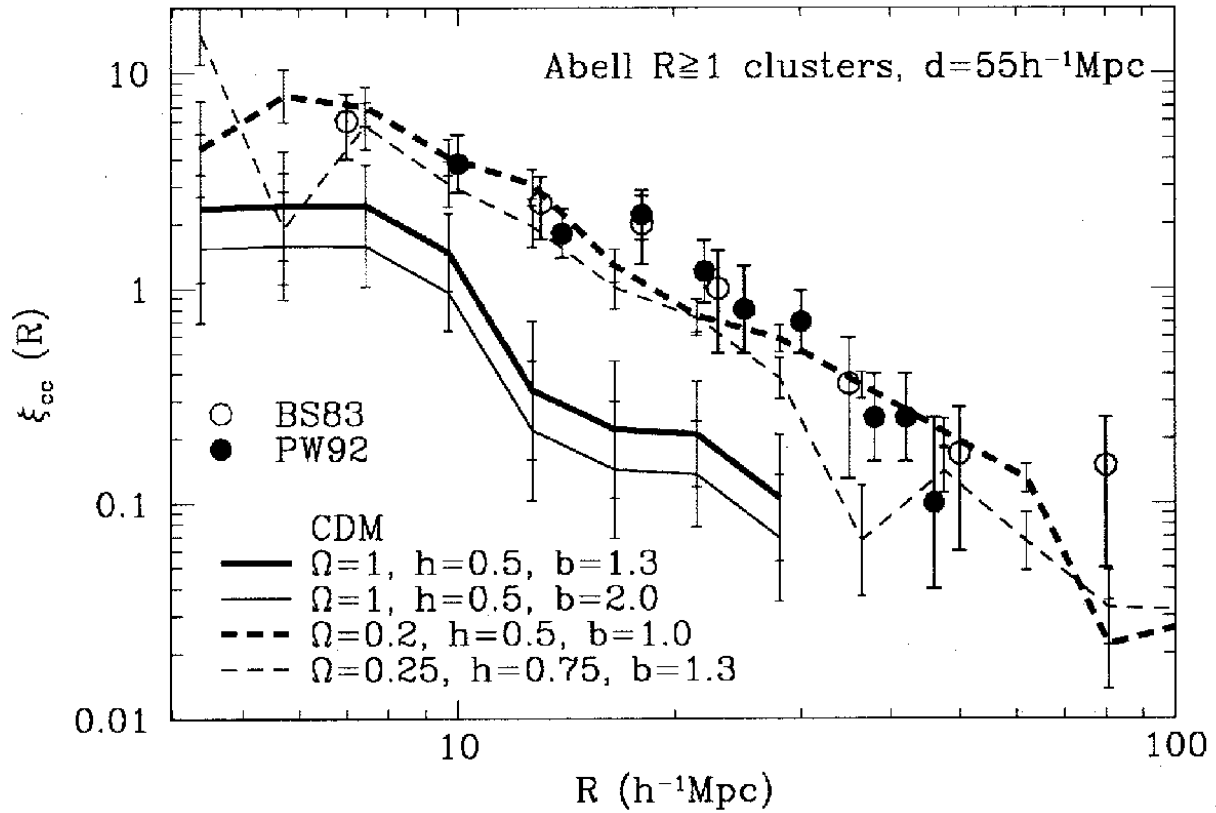


Fig. 9.— The correlation function of rich ( $R \geq 1$ ) Abell clusters, with  $d = 55h^{-1}$  Mpc, from observations 10, 43 and simulations 5.

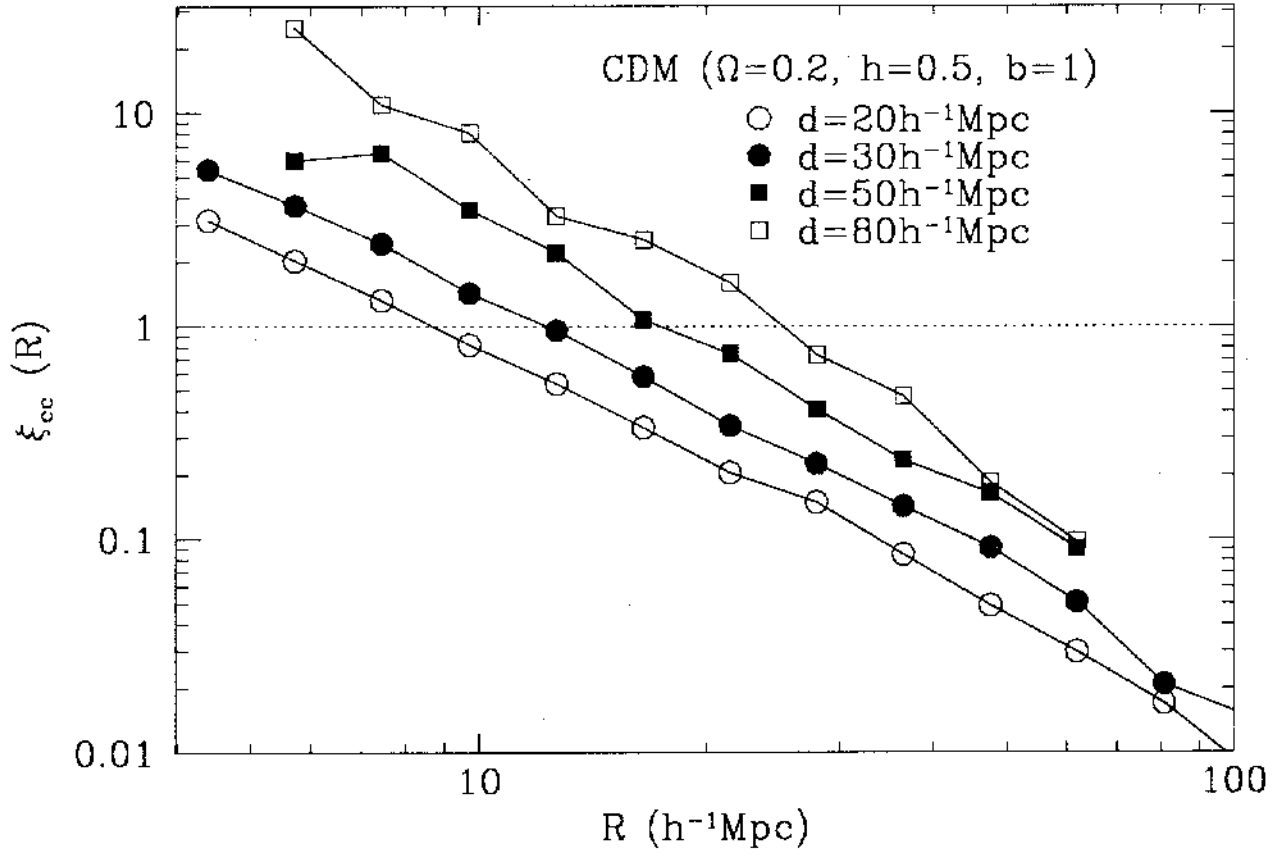


Fig. 10.— Dependence of the model cluster correlation function on mean cluster separation  $d$ .

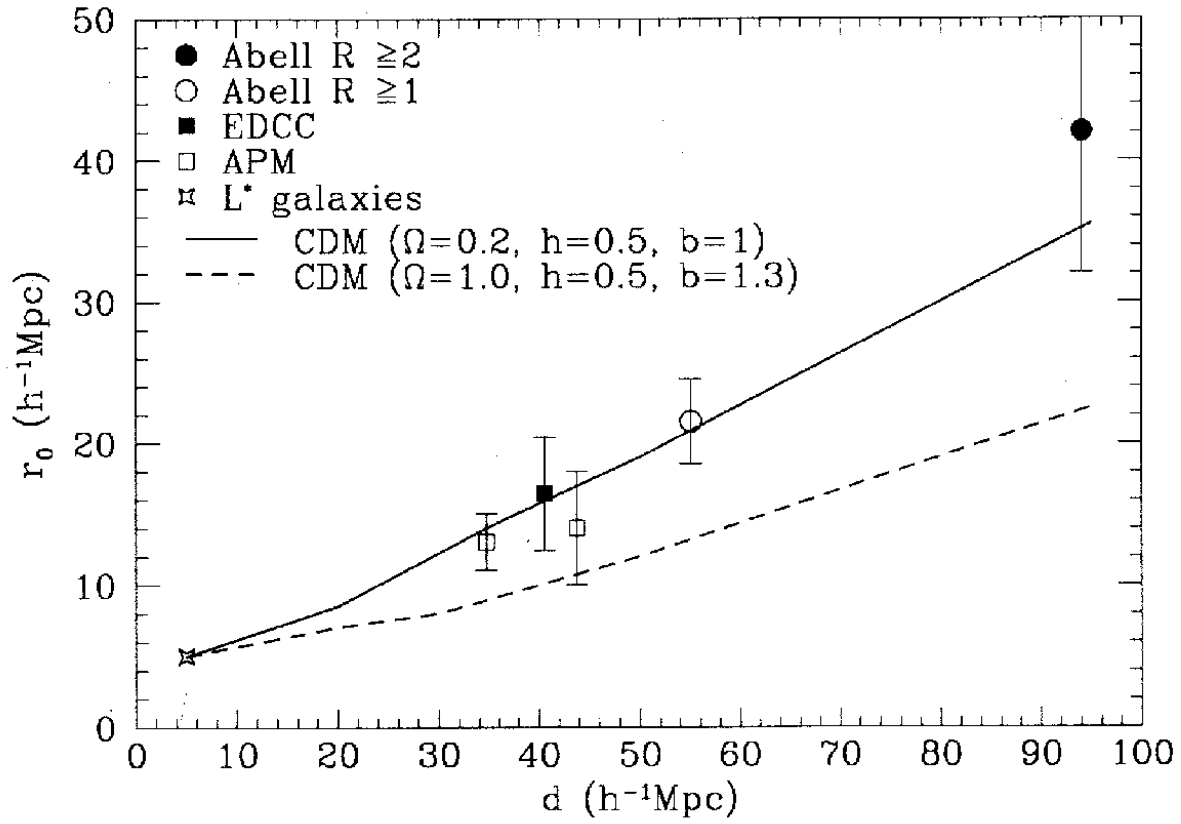


Fig. 11.— The correlation length of the cluster correlation function as a function of mean cluster separation, from observations and cosmological simulations 5.

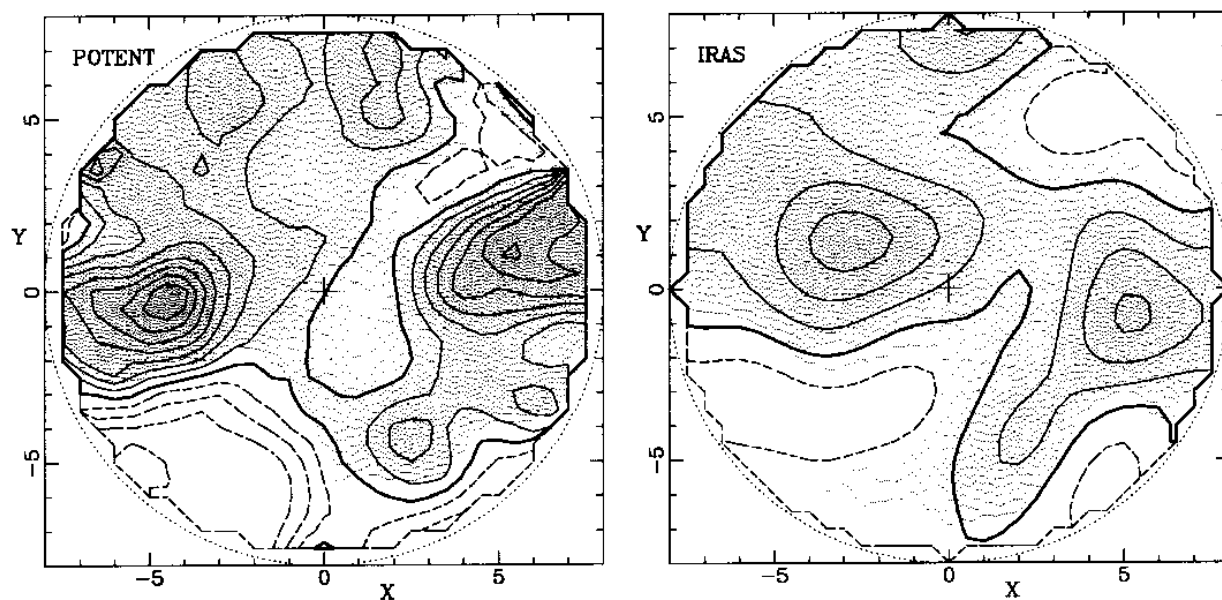


Fig. 12.— A comparison of the mass-density (reconstructed from velocity data) and galaxy-density fields. The left panel is the density field  $\nabla \cdot v$  in the supergalactic plane reconstructed from peculiar velocity data. The right panel is the independently determined density field of IRAS galaxies. The smoothing in both panels is  $1200 \text{ km s}^{-1}$ . The axes are labeled in  $1000 \text{ km s}^{-1}$ . The Local Group sits at the center of each panel (21, 52).

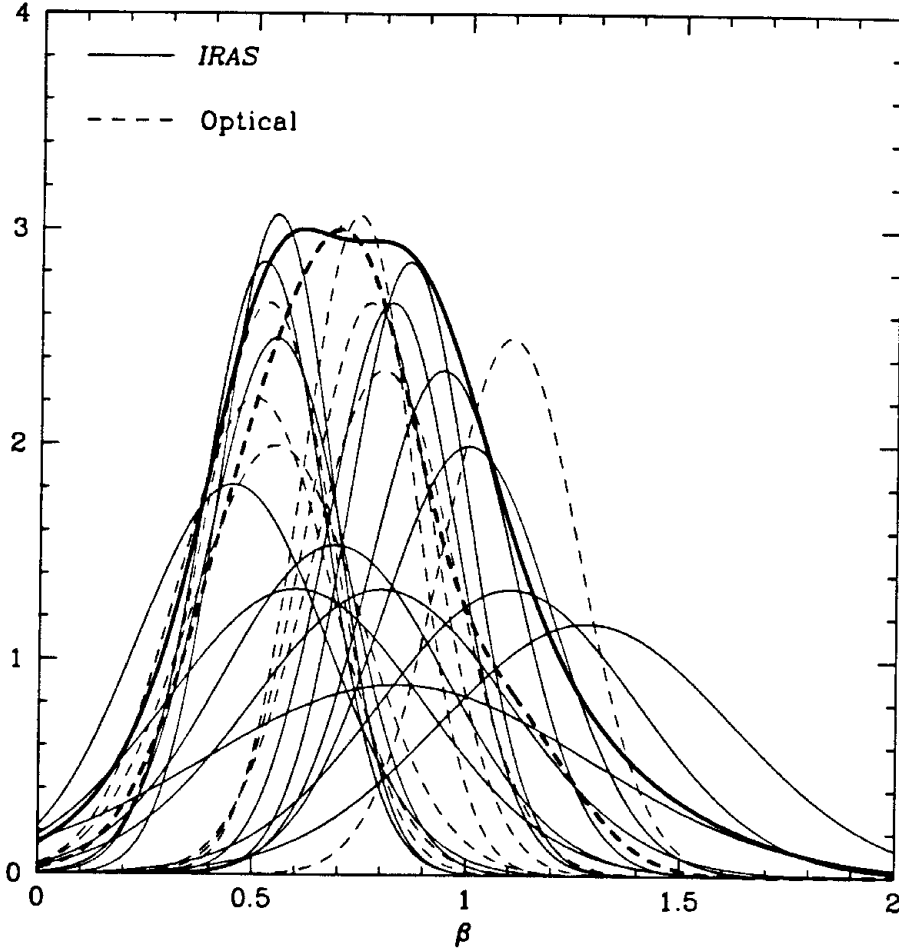


Fig. 13.— Distribution of  $\beta = \Omega_m^{0.6}/b$  determinations 52. Each measurement is shown as a Gaussian of unit integral with mean and standard deviations as given by the different observations. IRAS and optical determinations are plotted with different line types. The (renormalized) sum of all curves (optical and IRAS separately) are shown as the heavy curves.

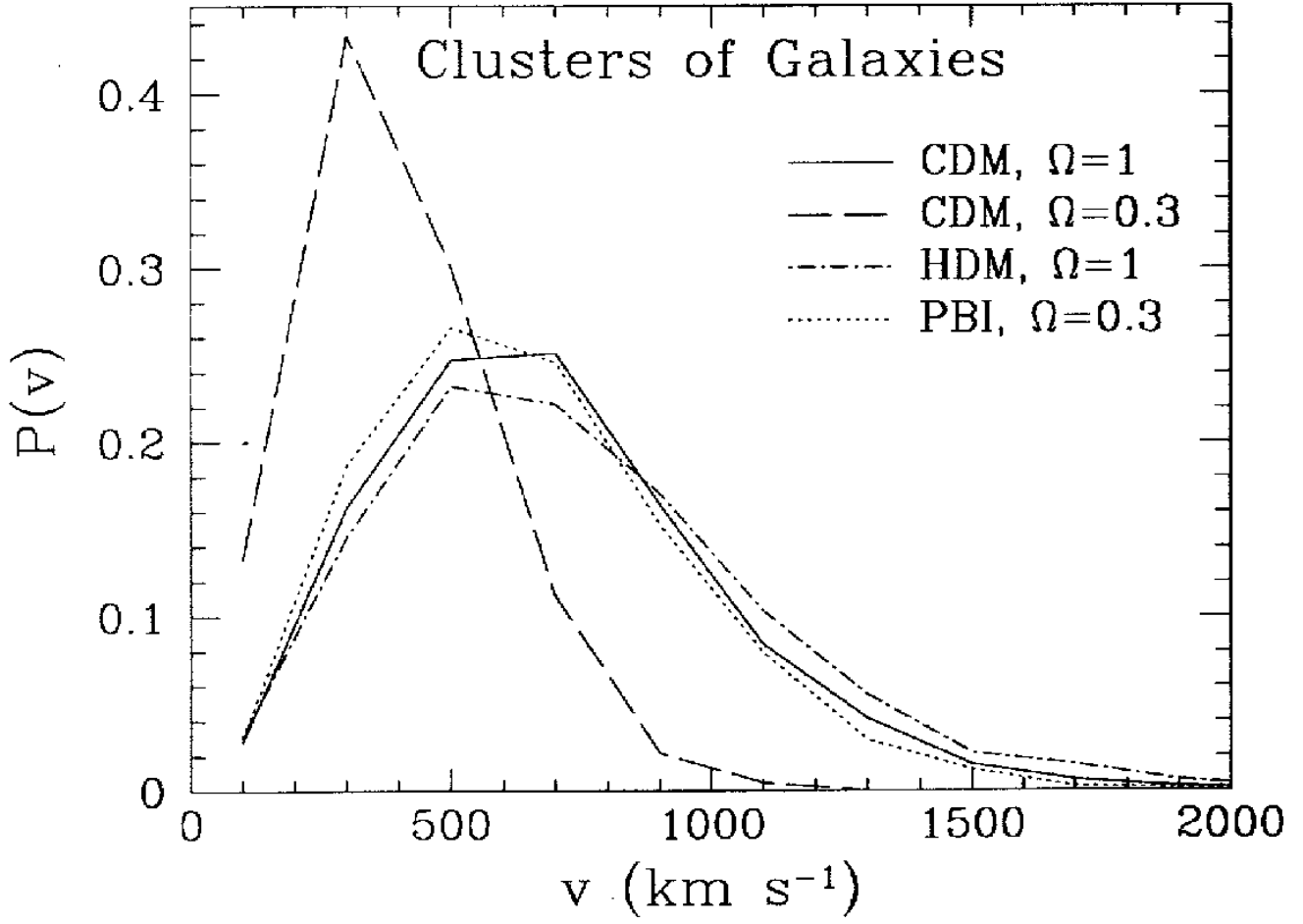


Fig. 14.— The cluster 3-D peculiar velocity distribution in four cosmological models 8.

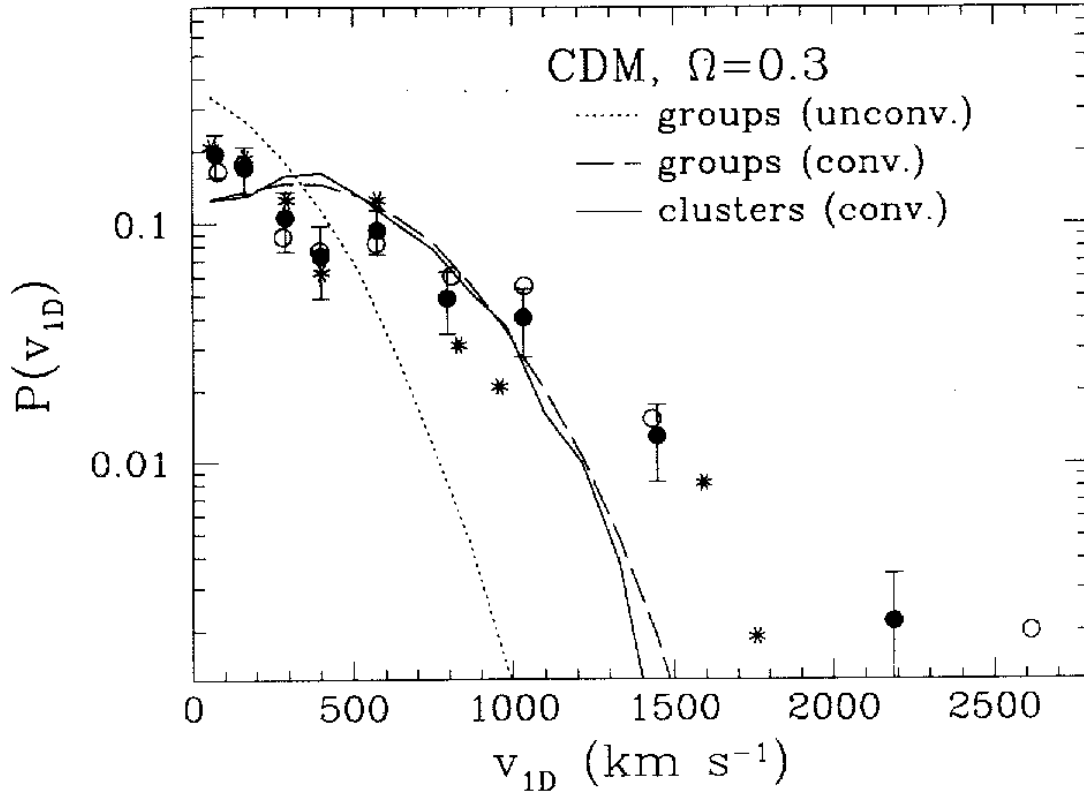


Fig. 15.— Comparison of the currently observed 1-D peculiar velocity distribution of groups and clusters of galaxies with expectation from an  $\Omega_m = 0.3$  CDM model. The dotted line is the model expectation; the dashed and solid lines are the model convolved with the observed velocity uncertainties 8.

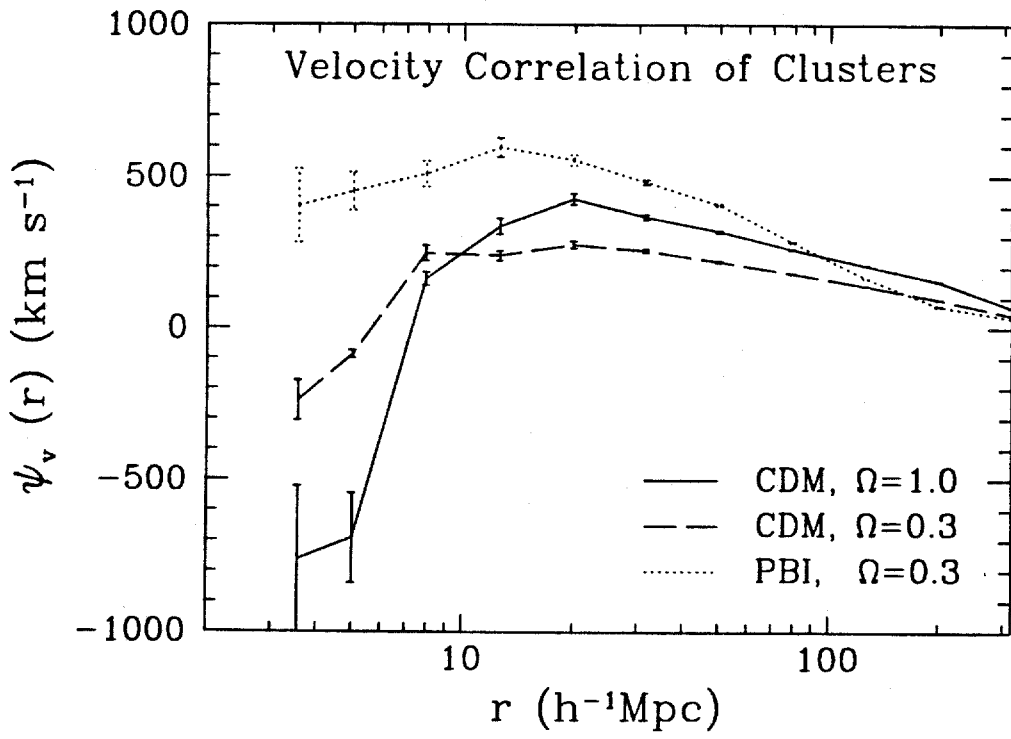


Fig. 16.— The velocity correlation function of rich ( $R \geq 1$ ) clusters for three models 15.

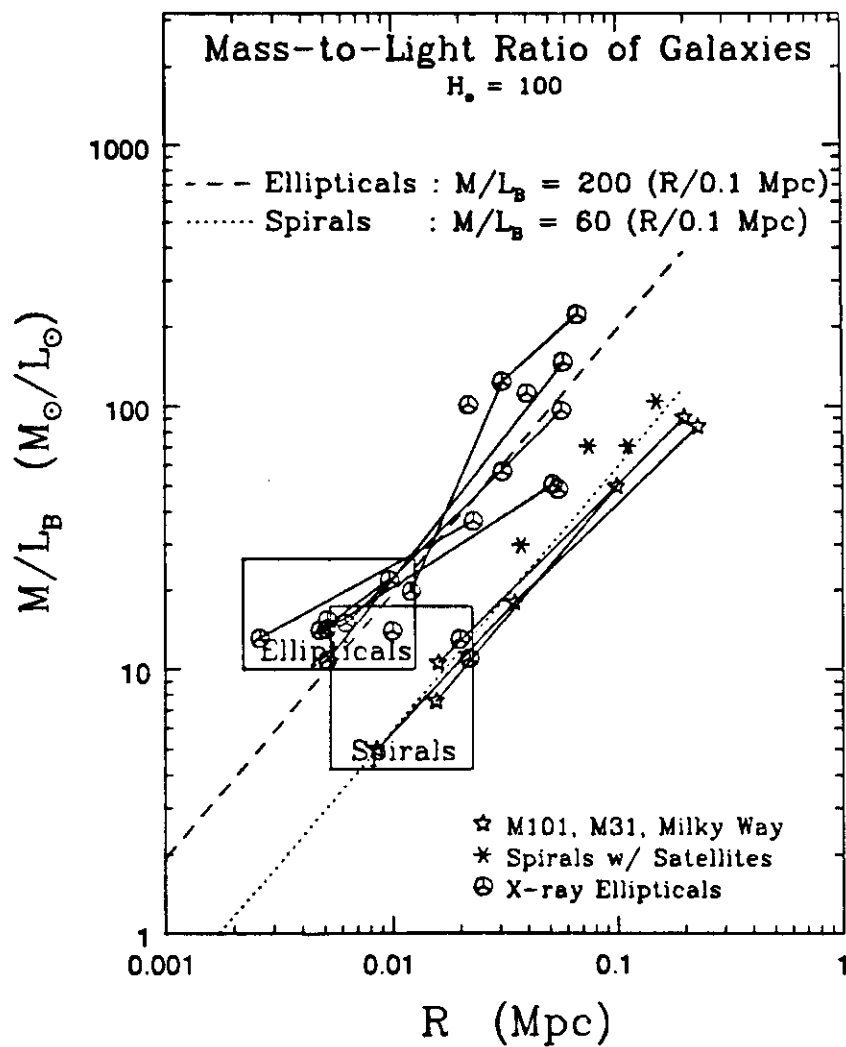


Fig. 17.— The mass-to-light ratio of spiral and elliptical galaxies as a function of scale. The large boxes indicate the typical ( $\sim 1\sigma$ ) range of  $M/L_B$  for bright ellipticals and spirals at their luminous (Holmberg) radii. ( $L_B$  refers to total corrected blue luminosity.) The best-fit  $M/L_B \propto R$  lines are shown 9.

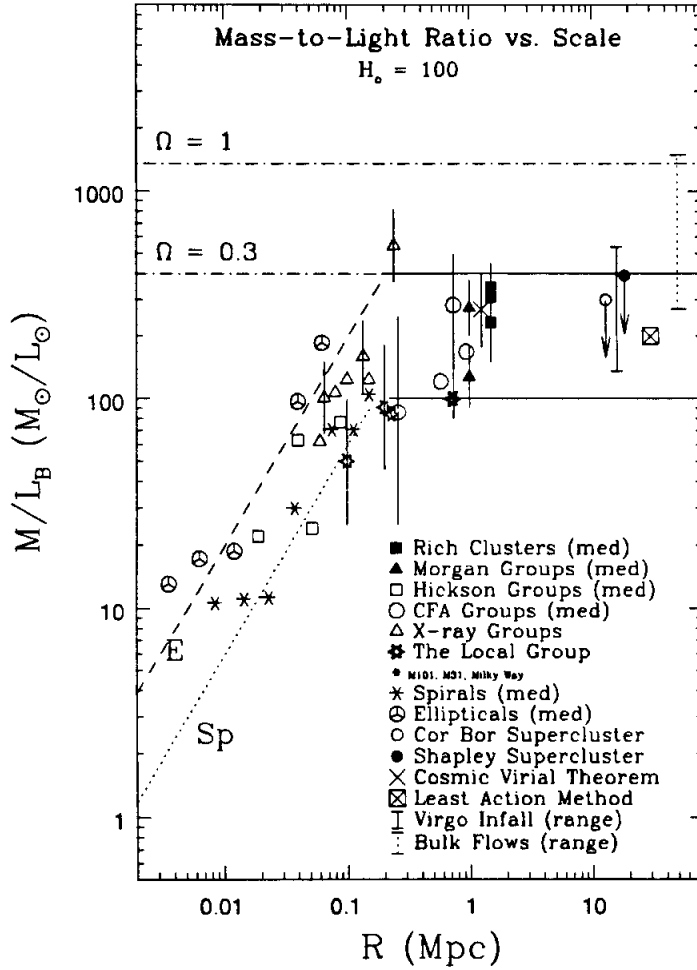


Fig. 18.— A composite mass-to-light ratio of different systems—galaxies, groups, clusters, and superclusters—as a function of scale. The best-fit  $M/L_B \propto R$  lines for spirals and ellipticals (from Fig. 17) are shown. Typical  $1\sigma$  scatter around median values are shown. Also presented, for comparison, are the  $M/L_B$  (or equivalently  $\Omega_m$ ) determinations from the Cosmic Virial Theorem, the Least Action method, and the range of various reported results from the Virgocentric infall and large-scale bulk flows (assuming mass traces light). The  $M/L_B$  expected for  $\Omega_m = 1$  and  $\Omega_m = 0.3$  are indicated.